Nanoscale

Laser nanobubbles induce immunogenic cell death in breast cancer

Journal:	*Nanoscale*
Manuscript ID	NR-ART-09-2020-006587.R1
Article Type:	Paper
Date Submitted by the Author:	23-Jan-2021
Complete List of Authors:	Nguyen, Hieu; The University of Texas at Austin, Biomedical Engineering Katta, Nitesh; The University of Texas at Austin, Electrical and Computer Engineering Widman, Jessica; The University of Texas at Austin, Biomedical Engineering Takematsu, Eri; The University of Texas at Austin, Biomedical Engineering Feng, Xu; Harvard Medical School Torres-Hurtado, Susana; The University of Texas at Austin, Biomedical Engineering Betancourt, Tania; Texas State University Baker, Aaron; The University of Texas at Austin, Biomedical Engineering Suggs, Laura; University of Texas at Austin Cockrell School of Engineering, Biomedical Engineering Milner, Thomas; University of California Irvine, Biomedical Engineering Tunnell, James; The University of Texas at Austin, Biomedical Engineering

ARTICLE

Laser nanobubbles induce immunogenic cell death in breast cancer†

Hieu T.M. Nguyen,[a] Nitesh Katta,[b] Jessica A. Widman,[a] Eri Takematsu,[a] Xu Feng,[a] Susana H. Torres,[a] Tania Betancourt,[c] Aaron B. Baker,[a] Laura J. Suggs,[a] Thomas E. Milner,[a,b] James W. Tunnell,[a]*

Received 00th January 20xx,
Accepted 00th January 20xx

DOI: 10.1039/x0xx00000x

Recent advances in immunotherapy have highlighted a need for therapeutics that initiate immunogenic cell death in tumors to stimulate the body's immune response to cancer. This study examines whether laser-generated bubbles surrounding nanoparticles ("nanobubbles") induce an immunogenic response for cancer treatment. A single nanosecond laser pulse at 1064 nm generates micron-sized bubbles surrounding gold nanorods in the cytoplasm of breast cancer cells. Cell death occurred in cells treated with nanorods and irradiated but not in cells with irradiation treatment alone. Cells treated with nanorods and irradiation had increased damage-associated molecular patterns (DAMPs), including increased expression of chaperone proteins human high mobility group box 1 (HMGB1), adenosine triphosphate (ATP), and heat shock protein 70 (HSP70). This enhanced expression of DAMPs led to the activation of dendritic cells. Overall, this treatment approach is a rapid and highly specific method to eradicate tumor cells with simultaneous immunogenic cell death signaling, showing potential as a combination strategy for immunotherapy.

Introduction

Immunotherapy has become the primary treatment for several advanced, metastatic cancers including melanoma, lung cancer, and head and neck cancers.[1–4] Despite the success of immunotherapy, the proportion of patients that do not respond or have incomplete responses to the therapy are high for many types of cancer.[3,5,6] The reason for these low response rates is believed to be that tumors produce immunosuppressive factors that prevent immune recognition and tumor cell death.

A key strategy to enhance immunotherapy is to elicit immunogenic cell death in tumor cells. Immunogenic cell death results in both antigenicity (release of tumor-specific antigen) and adjuvanticity (release of molecular signaling that stimulates immune responses). Adjuvant signaling by the secretion of damage-associated molecular patterns (DAMPs) has been shown to activate dendritic cells to acquire tumor-specific antigens that mount adaptive T cell responses specific to tumor cells.[7–10]

Targeted hyperthermia (locally controlled tumor radiative heating with laser and nanoparticles[11–14]) has emerged as a promising therapeutic approach that elicits immunogenic tumor cell death.[15–20] Most recently, the synergy between hyperthermia therapy and immunotherapy (immune checkpoint and adoptive T cell therapy) was demonstrated in pre-clinical models illustrating that, when combined with hyperthermia, tumor burden was minimized over any monotherapy.[21–23]

Laser nanobubbles (bubbles generated around nanoparticles from irradiation with nanosecond pulsed laser radiation) offer an alternative method to trigger cell death via physical disruption of cell membranes. This mechanism leads to a necrotic cell death fate[24] with the potential to elicit more inflammatory, pro-immunogenic signaling. The secretion of immunogenic markers into the extracellular environment by laser nanobubbles occurs in binary events and without strong dependence on dosimetry. Therefore, they eliminate the need for a dosimetry monitoring system during laser treatment. Moreover, laser nanobubbles can trigger cell death after one pulse of laser irradiation,[24–27] while targeted hyperthermia typically requires a few minutes to deliver the optimal temperature.[11] The rapid therapeutic creation of laser nanobubbles may facilitate the treatment of large tumors.

In this study, we demonstrate immunogenic cell death from laser nanobubbles for the first time. Following a single nanosecond laser pulse irradiation, rapid breast cancer cell death occurred due to membrane disruption. Moreover, this effect was highly specific, causing membrane disruption only in cells with gold nanorods (AuNRs), while neighboring cells without AuNRs were left intact. We also observed bubble formation in cells, confirming the AuNRs-laser interaction is transient and discrete. We determined that extracellular release of DAMPs, including chaperone proteins, human high mobility group box 1 (HMGB1), adenosine triphosphate (ATP), and heat shock protein 70 (HSP70) were enhanced in the laser

[a] Department of Biomedical Engineering, The University of Texas at Austin, TX, USA
[b] Department of Electrical and Computer Engineering, The University of Texas at Austin, TX, USA
[c] Department of Chemistry and Biochemistry, Texas State University, TX, USA
* Correspondence email: jtunnell@mail.utexas.edu

† Electronic Supplementary Information (ESI) available: Details about the laser beam profile, calreticulin redistribution from nanobubbles, dendritic cell maturation induced from the supernatant of treated groups, and gating strategy. See DOI: 10.1039/x0xx00000x

treatment group. With the presence of DAMPs secreted from laser irradiation, dendritic cell activation increased. Overall, we demonstrated that nanosecond pulsed laser irradiation provided a fast and highly specific therapy to eradicate tumor cells and elicit immunogenic cell death, highlighting the potential of this approach as a candidate combination strategy for immunotherapy.

Results and discussion

We used AuNRs coated with (11-Mercaptoundecyl)-N,N,N-trimethylammonium bromide (Mutab), a quaternary ammonium compound that is capable of driving cellular uptake due to their positive zeta potential.[28,29] The AuNRs were 38 nm long and 10 nm wide (aspect ratio of 4:1) and had a peak surface plasmon resonance (SPR) at 788 nm (Figure 1a). Laser irradiation at 1064 nm only results in 25% absorption of the SPR peak at 788 nm. While the longitudinal SPR peak of AuNRs can be tuned to match the laser irradiation by increasing the AuNRs aspect ratio, cellular uptake significantly reduces with increasing AuNR length.[30–32] This off-resonance absorption can be compensated by radiation with higher fluence while maintaining a significant margin between triggering cell death with and without AuNRs.[26] The metabolic activities of human and murine breast cancer cells (MDA-MB-231 and 4T1 cells) were characterized by the tetrazolium compound [3-(4,5-dimethylthiazol-2-yl)-5-(3-carboxymethoxyphenyl)-2-(4-sulfophenyl)-2H-tetrazolium (MTS) assay. The metabolic activities of cells incubated with AuNRs within 3, 6, 12, and 24 hours were similar to that of cells without AuNRs (Figure 1b). Hence, AuNRs have minimal cytotoxicity on MDA-MB-21 and 4T1 cells. Two-photon microscopy images of AuNRs internalization in MDA-MB-231 and 4T1 cells shows the uptake of AuNRs for 6 hours (Figure 1c). The cytoplasm of live cells stained with calcein-AM appears in green, while AuNRs clusters photo-luminesce over a broad spectrum and appear in yellow as a result of the overlapping of red and green channels. The internalized AuNRs cluster in various sizes and appear randomly distributed in the cytoplasm.

We determined the fluence threshold required for cell membrane disruption using calcein-AM and ethidium homodimer-1 (EthD-1) staining. The polyanionic calcein-AM can permeate through the membrane of live cells and produce an intense uniform green fluorescence in live cells. On the contrary, EthD-1 enters cells with damaged membranes, binds to nucleic acids, and provides a bright red fluorescence in dead cells. Figure 2a displays two-photon images of cells incubated with AuNRs after single-pulse nanosecond laser treatment at different fluences (0.7-5 J/cm^2). We observed that the area of cell death occurs at the beam center at lower fluence and expands outwards from the beam center as laser fluence increases. The laser beam profile is approximately Gaussian (Figure S1); therefore, the ablation threshold is first exceeded in the beam center. The beam shape is not a perfect Gaussian and likely results in the observed irregularity in cell death areas. The fluence threshold required for membrane disruption is between 0.7 to 1.5 J/cm^2, an order of magnitude higher than that reported in the literature[24] of 0.07 J/cm^2. This is likely a result of the 1064nm laser wavelength used here that operates off the resonance peak of the AuNRs at 788 nm. The damage threshold

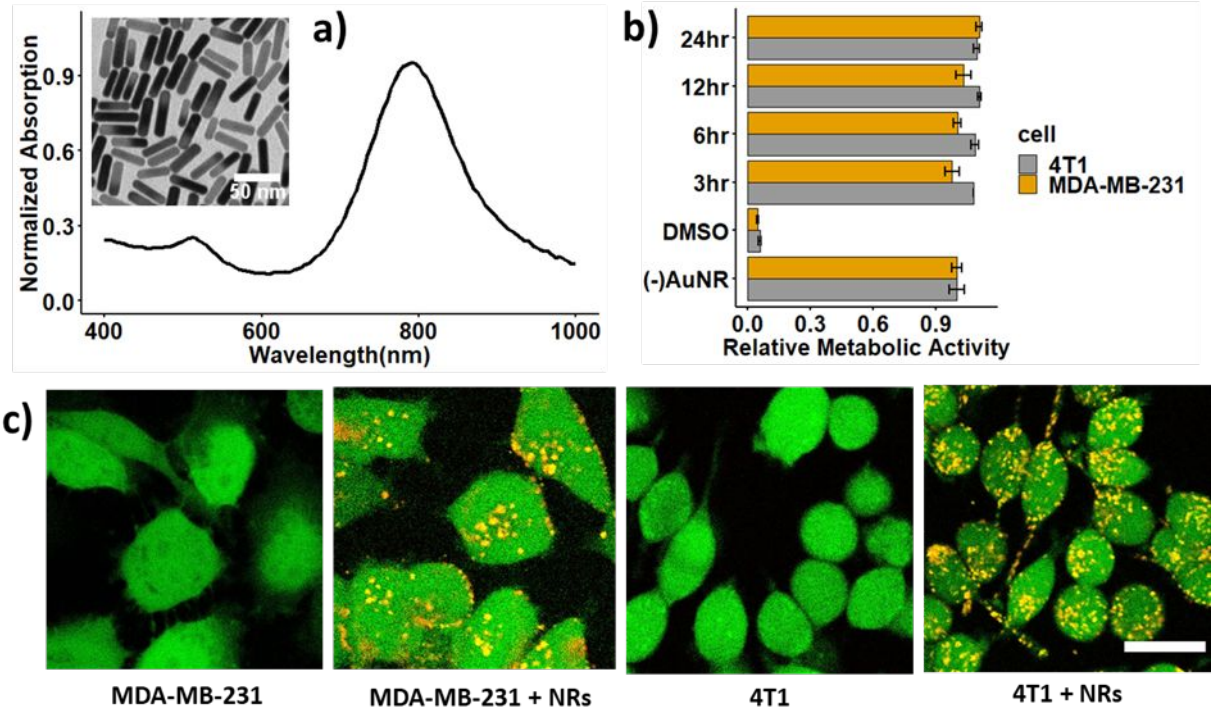

Figure 1 Gold nanorods (AuNRs) internalization in breast cancer cells: a) absorption spectrum of Mutab-coated AuNRs and TEM image of the nanorods (insert); b) relative metabolic activity of 4T1 and MDA-MB-231 cells incubated with AuNRs; c) two-photon images of MDA-MB-231 and 4T1 cells without and with AuNRs incubated for 6 hours. Scale bar: 20 µm

for cells without AuNRs is likely much higher, above 5 J/cm^2, as we did not observe dead cells at this fluence (data not shown). We found a similar trend in 4T1 cells reported previously, where a fluence threshold for membrane disruption in cells with AuNRs is between 0.7 to 1.5 J/cm^2, and the cell death area expands with increasing laser fluence.[33]

To examine the specificity of laser treatment, we prepared three types of MDA-MB-231 cell populations: (a) without AuNRs, (b) with AuNRs, and (c) co-cultured cells with and without AuNRs at the ratio of 2:1. We irradiated cells at 3 J/cm^2, followed by calcein-AM and EthD-1 staining (Figure 2b-c). We observed 0.3% of dead cells in the center of the beam for cells irradiated in the absence of AuNRs, 99% of dead cells for cells cultured with AuNRs, and 63% of dead cells for the group containing cells with and without AuNRs (Figure 2d). These percentages of cell death match well to the percentage of cells with AuNRs in the samples and demonstrate that within the laser beam, only AuNR-embedded cells were found dead while neighboring cells without AuNRs were intact. This observation is consistent with Pitsillides et al., who observed membrane disruption on cells with microparticles after nanosecond laser irradiation, while adjacent cells without microparticles were undamaged.[25] These results imply that this laser treatment is highly specific, affecting only the cells in direct contact with the AuNRs.

We visualized AuNRs-laser interaction in 4T1 cells using the custom inverted microscope setup shown in Figure 3a. The 1064 nm excitation laser beam was focused to a spot of 60 µm (full width half maximum) on the mono-layer 4T1 cells through the microscope objective (40x). The diffraction limit of the system is calculated at 0.26 µm. We used a high-speed camera (25,000 frames per second) to record videos of cells after single-pulse irradiation at 3 J/cm^2 (supplemental video V1, V2; selected frames Figure 3b). The bubbles scatter light; hence, they appear as dark regions in image frames. We observed multiple bubbles expanding and collapsing on cells with AuNRs. Bubble diameters ranged between 0.8 and 3 µm (Figure 3b). No bubbles were observed after laser irradiation of cells without AuNRs (data not shown). Theoretical models and experimental measurements previously reported that nanosecond laser irradiation of single nanoparticle results in the generation of 0.1 - 0.5 µm bubbles.[34–36] The larger bubbles we observed may be due to AuNR clusters resulting from cell internalization. The bubble formation is evidence of the transient AuNRs absorption of the high energy laser pulse, which is then converted to mechanical disruption forces (high pressure and temperature) in cells. Moreover, these disruption forces are localized at the micrometer scale around AuNRs, which explains the high specificity of laser irradiation observed in Figure 2b-d.

We examined the bubble lifetime by monitoring the mean intensity of the bubble dark pixels over time (Figure 3c). At the

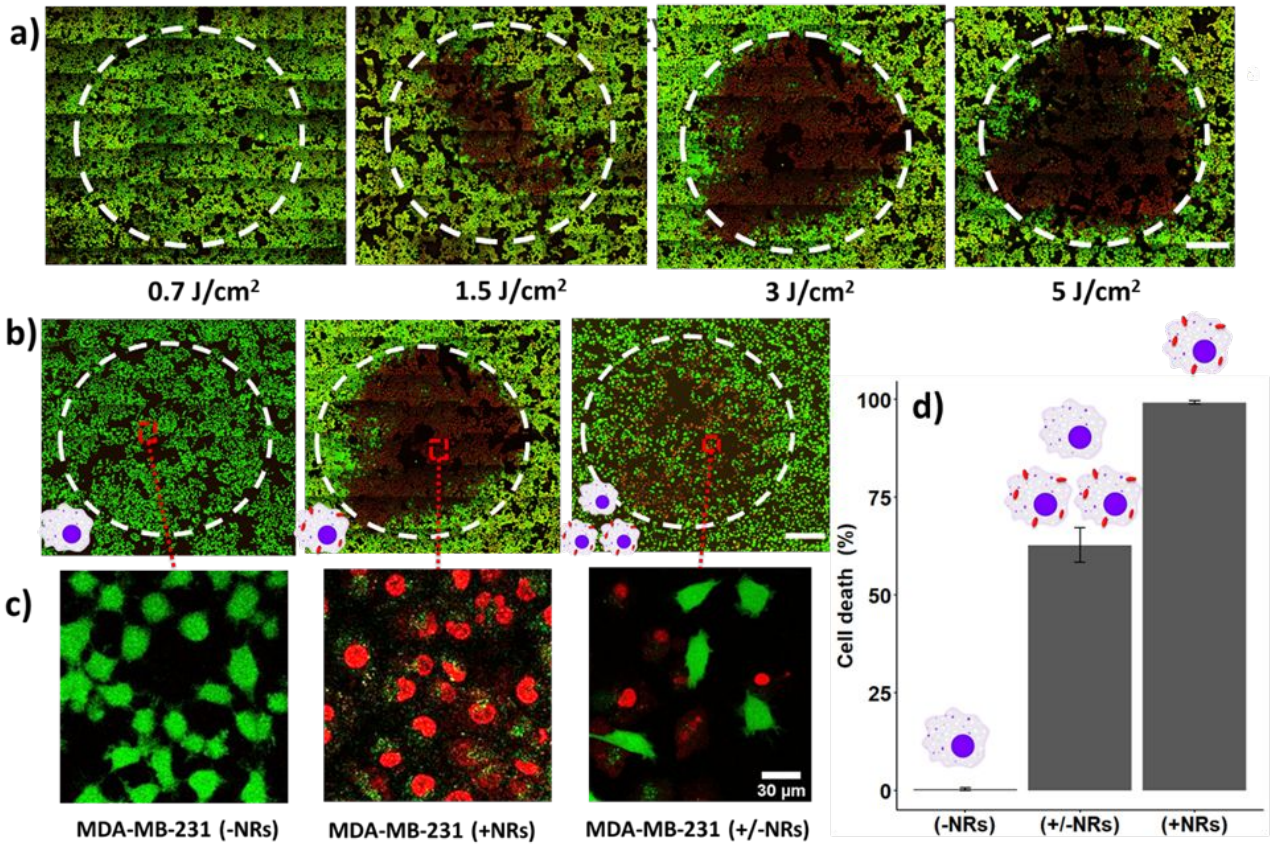

Figure 2 Cell death resulting from laser (1064 nm) irradiation of AuNRs-incubated MDA-MBA-231 cells: a) cell death with varying fluence from 0.7-5 J/cm^2; b-d) cell death specific to irradiation of AuNRs-embedded MDA-MBA-231 cells at 3 J/cm^2: without AuNRs incubation (left), with AuNRs incubation (middle) and with a mix of these two populations in 2:1 ratio (right). A two-photon microscope acquires the images with live cells stained in green (calcein-AM) and dead cells stained in red (ethidium homodimer-1). Beamwidth is highlighted with a white dashed line. Scale bar: 0.5 mm

time of laser irradiation, we observed a surge of intensity due to laser flash, followed by an instant sharp drop of intensity as the bubble formed. As the bubble collapsed, fewer dark pixels were present and the mean intensity recovered following a polynomial function as described in previous theoretical models studying gas bubble dissolution in liquid medium.[37–40] Zhang et al. derived the lifetime of a nanobubble τ as a function of its original radius R_0 as follows[39]

$$\tau = \frac{R_0^3 \quad \rho_g}{6KD\gamma_0\left(1-\frac{\rho_g}{\rho_l}\right)^4}$$

Where K is Henry's law constant representing the gas solubility in liquid, D is the diffusion coefficient of the gas in the liquid, γ_0 is the surface tension of liquid on a macroscopic scale, ρ_g and ρ_l are the density of gas and liquid, respectively. The lifetime of the bubbles recorded in cells (time that bubble intensity increases 1/e of its minimum-to-plateau difference) increased with the bubble's diameter following a polynomial expression as described above (Figure 3d). We also observed that the bubble's lifetimes are on the order of milliseconds, which are three orders of magnitude longer than the lifetime of similar-size bubbles in water (~300 ns) reported previously.[34,36,41] The long lifetime of bubbles in cells can be explained by the low gas solubility and diffusion coefficient in the cytoplasmic fluid. As cytoplasm fluid contains large biomolecules, its solubility of gases in it is expected to be much lower than that in water.[42] Furthermore, cytoplasmic diffusion of oxygen is two orders of magnitude lower than oxygen diffusion in water (~50 μm²/s in cytoplasmic fluid vs. 2500 μm²/s in water).[43] While the inverted microscope images reveal the formation and collapse of bubbles in cells, we cannot confirm the onset of membrane disruption with the system. The cell membrane disruption observed in Figure 2 is likely the result of cavitation erosion, which occurs when bubbles collapse, generating re-entrant jet dynamics and emitting shock waves,[44,45] creating damage on the cell membrane.

To examine whether the nanobubbles can trigger immunogenic cell death, we characterized the release of damage-associated patterns (DAMPs) including heat shock protein 70 (HSP70),

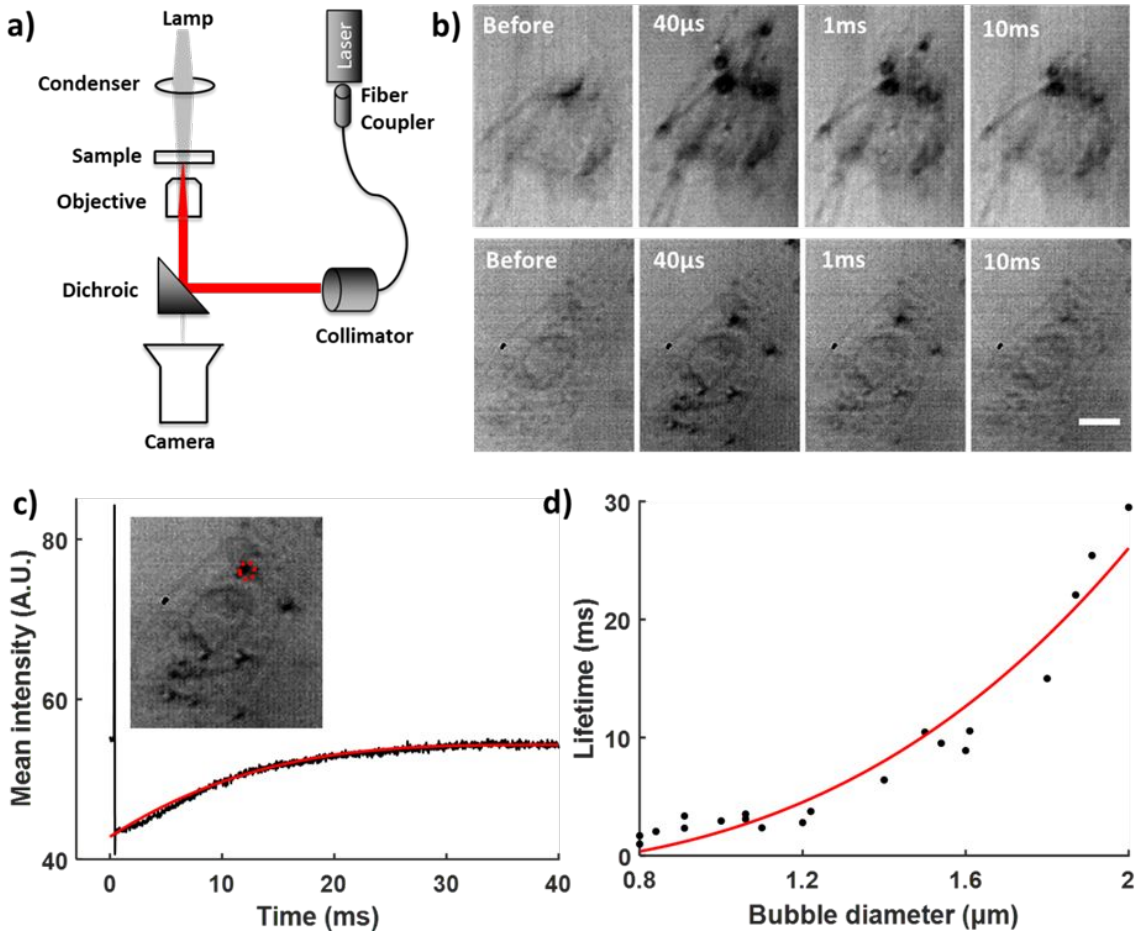

Figure 3 Imaging bubbles following rapid heating and water vaporization around AuNRs. (a) Assembly of the optical system to image bubbles, (b) montage of bubbles formed in two examples of 4T1 cells embedded with AuNRs after one pulse of laser irradiation at 3 J/cm², (c) mean intensity of bubble over its time course with polynomial fitting (red line), the red dash line highlights the bubble pixels being monitored, (d) bubble's lifetime vs. diameter with polynomial fitting (red line). Scale bar: 10 μm

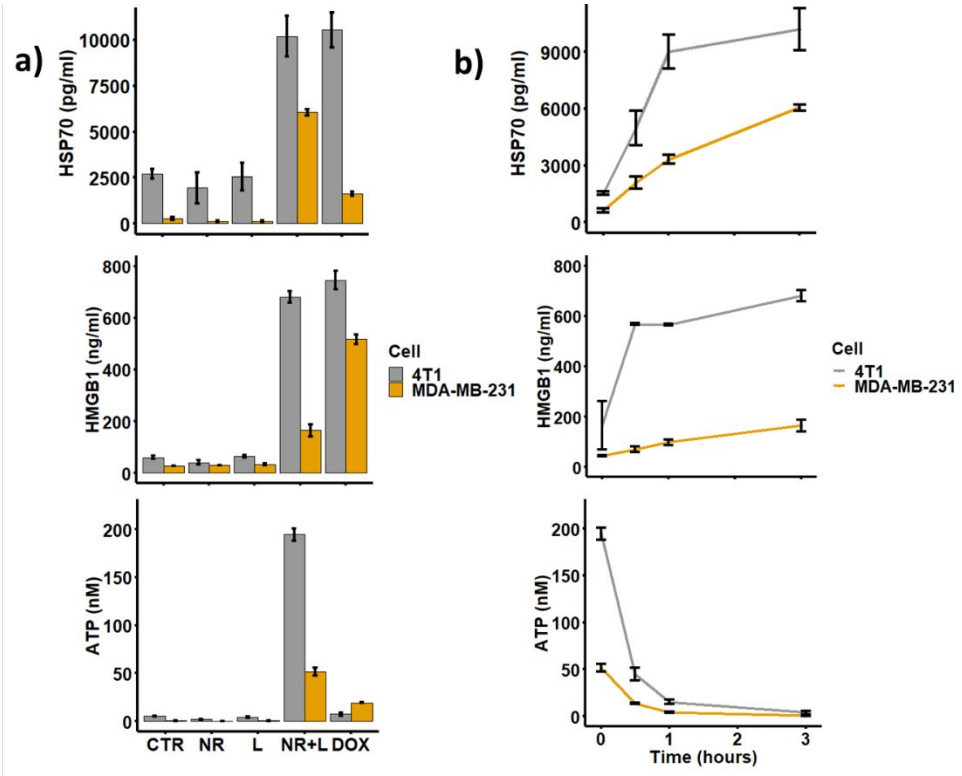

Figure 4 Extracellular release of damage associated patterns from laser irradiation of MDA-MB-231 and 4T1 cells at 3 J/cm² and 2 cm² of cells area per sample (50% of the well area), a) HSP70, HMGB1, and ATP; b) Time-dependent release of DAMPs after laser irradiation. Groups: CTR: cells without any treatment, NR: cells incubated with AuNRs, L: cells irradiated with a laser, NR+L: cell incubated with AuNRs and irradiated with a laser, DOX: cell treated with doxorubicin for 24 hours as the positive control. The number of samples per group n = 3

chaperone protein human high mobility group box 1 (HMGB1) and adenosine triphosphate (ATP) in the extracellular environment by ELISA and bioluminescence assays (Figure 4). Several damage-associated molecular patterns (DAMPs) have been identified for immunogenic cell death confirmation, including ATP, HMGB1, chaperone calreticulin, HSP family, immune cytokines, sphingomyelin metabolites, mitochondrial products, cytosolic components and product of extracellular matrix breakdown.[7] Here, we studied four types of DAMPs (ATP, HMGB1, chaperone calreticulin, HSP70) that have been widely recognized for their key role in immunogenic response in most immunogenic cell death inducers.[7–9,46] The MDA-MB-231 and 4T1 cells were treated with Doxorubicin 1 µg/ml and 10 µg/ml, respectively, for 24 hours as a positive control. We observed increased release of all three types of DAMPs in both cell lines in groups with AuNRs and laser irradiation. The 4T1 cells released more DAMPs than the MDA-MB-231 due to its higher metabolic activity. We also observed two trends of DAMPs secretion: the release of HSP70 and HMGB1 increased with time while the ATP quenched quickly with time (Figure 4b). After membrane disruption from laser irradiation, the DAMPs proteins were released gradually into the extracellular environment as cells follow the necrosis pathway. On the contrary, most ATP molecules inside the cells were secreted immediately after laser irradiation. These ATP molecules were unstable in the extracellular environment and hence, were quickly lessened after one hour. Laser irradiation triggered ATP release instantly, creating a surge of ATP in the extracellular environment in contrast with doxorubicin treatment, where ATP was released gradually. As a result, we observed a much higher amount of ATP in the laser-treated group than the doxorubicin-treated group at the time of measurement. We characterized calreticulin relocation in MDA-MB-231 as a signal of immunogenic cell death with confocal fluorescence imaging (Figure S2). We labelled the cell nucleus with Hoechst (blue), cell membrane with Cellmask (green), and calreticulin with AF647 conjugated antibodies (red). We observed enhanced expression of calreticulin of positive control (cell incubated with Doxorubicin) whereas the dying cells from laser treatment shrank and caused calreticulin overlapped with the cell membrane.

To verify whether dendritic cells are activated with the presence of DAMPs signals released from laser irradiation, we co-cultured 4T1 cells and dendritic cells (DCs) in a trans-well system (Figure 5a). Bone marrow-derived dendritic cells (DCs) from BALB/c mice housed were cultured as per the Lutz method, with the addition of IL-4.[47–49] A significant increase in the percentage of mature DCs (Cd11c+ MHCII+ and CD86+) was observed in a group of laser irradiation of AuNRs-embedded 4T1 cells (Figure 5b, c). This increase is mostly driven by an upregulation in major histocompatibility complex (MHCII), which increases several folds during dendritic cell maturation.[50] We did not observe an increase in the percentage of mature dendritic cells when the 4T1 cells with AuNRs were irradiated for one time. We believe the ratio of 4T1 cells over DCs is crucial for activating DCs from DAMPs. This ratio is very skewed towards tumor cells in vivo as

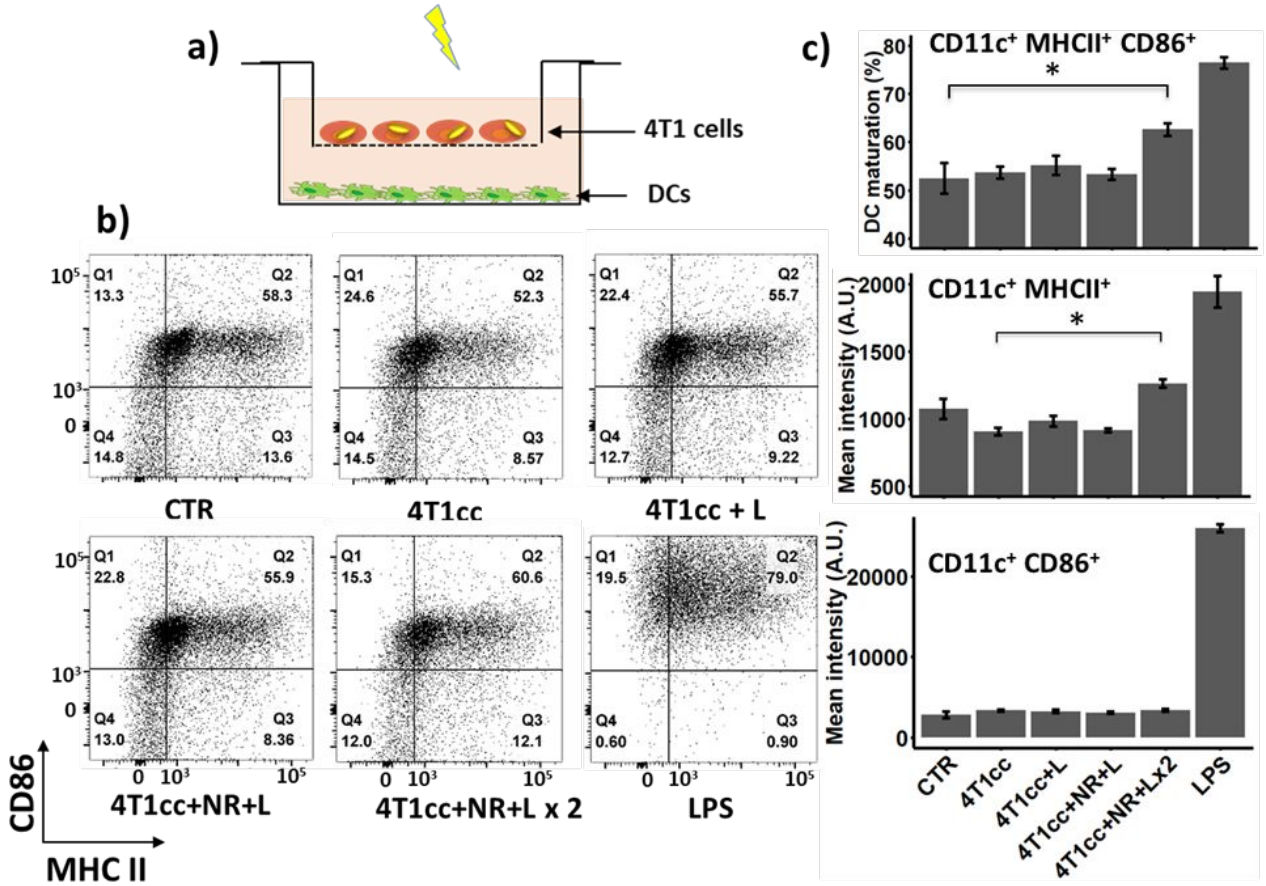

Figure 5 Activation of dendritic cells from irradiation of AuNRs-embedded 4T1 cells a) experimental layout describing 4T1 co-cultured with DCs in a transwell setting, b) Dot plot of DCs expressing MHC II and CD86, c) Percentage of mature dendritic cells as CD11c+ MHCII+ and CD86+, and median intensity of DCs that express MHCII and CD86. Six groups of dendritic cells: CTR: DCs without treatment; 4T1cc: DCs co-cultured with 4T1 cells; 4T1cc+L: DCs cultured with irradiated 4T1 cells; 4T1cc+NR+L: DCs co-cultured with irradiated AuNRs-embedded 4T1 cells; 4T1cc+NR+L x 2: DCs co-cultured with twice irradiated AuNRs-embedded 4T1 cells, the second irradiation is 12 hours after the first irradiation; LPS: DCs treated with LPS at 1 μg/ml for 12 hours. Number of samples per group n = 3. Statistical analysis was performed with analysis variance (ANOVA) in combination with Tukey test, * means p-value < 0.05

DCs are rare population in tissue (<1%),[51] while our simulated experiment is oppositely skewed due to the design of the transwell system (one 4T1 cell per DC). By irradiating 4T1 cells incubated with AuNRs more than once, more DAMPs per DCs are attained, thus increase the chance of activating DCs. We expect a more favorable outcome in vivo experiments because the ratio of DAMPs per DC will be significantly higher. We also observed enhanced dendritic cell activation with AuNRs and laser treatments of 4T1 cells in a different experimental setting where we incubated the dendritic cells with the supernatant from 4T1 cells culture medium instead of using trans-wells (Figure S3). The enhanced expression of mature dendritic cell markers CD80 and CD86 were significantly different with control groups when 4T1 cells were treated with AuNRs and laser (Figure S3c). We opted to study dendritic cells activation from DAMPs signal released from 4T1 cells (murine cell line) as a representative model to illustrate the proof of concept on whether the nanobubbles can trigger an immune response in vitro. These results can guide future experiments to study the immune response of nanobubbles in vivo within a BalB/C mouse model. We also recommend future studies to consider multiple pulses and different frequency of pulses to optimize the release of immune markers in breast cancer cells.

Experimental

Cell culture

Human breast cancer cells (MDA-MB-231) and murine breast cancer cells (4T1) were originally obtained from the American Type Culture Collection (ATCC). Both cell lines were seeded in T25 flasks with cell culture media composed of Dulbecco's Modified Eagle's Medium supplemented with 1% penicillin, 1% glutamine, and 10% fetal bovine serum (Sigma-Aldrich) in a humidified incubator at 37 °C under a 5% CO2 atmosphere. When cells reached confluence, they were seeded to either sterile 18mm coverslips (Electron Microscopy Science) for imaging or to cell culture plate (Cell Treat) for assays.

AuNRs internalization

AuNRs internalization into cells was determined using two-photon imaging. MDA-MB-231 and 4T1 cells were incubated with 35μg/ml (11-Mercaptoundecyl)-N,N,N-trimethylammonium bromide (Mutab) coated AuNRs (Nanopartz, 38nm long, 10nm diameter, pH = 7, zeta potential: +35 mV, surface plasmon resonance peak: 788 nm) in 1 ml culture medium for 6 hours. The cytoplasm of cells was stained with Calcein AM (Invitrogen) following the staining protocol from the supplier. AuNRs in cells were imaged with two-

photon microscopy (Prairie Technology), as detailed by Pattani.[52] Briefly, the laser of the two-photon microscope was tuned to 780nm to image both the AuNRs and Calcein AM. We used a 595+/-50nm bandpass filter to capture calcein-AM's florescence. AuNRs photo-luminesce in a broad spectrum[53] and were detected through the 595+/-50nm and the 660 +/-20 nm bandpass filters.

Cytocompatibility of AuNRs

For cytotoxicity assessment of gold nanorods, MDA-MB-231 and 4T1 cells were seeded onto a 96-well plate at a cell density of 5,000 cells per well and grown for 24 hours prior to the addition of AuNRs. The cells were incubated with AuNRs for 3, 6, 12, and 24 hours at 35μg/ml in culture media. Cells incubated with DMSO for 20 minutes were prepared as a positive control. After the incubation time, the AuNRs suspensions and DMSO were removed, and the cells were washed once with phosphate-buffered saline (PBS). We then added 20μl of MTS agent (Promega) into each well containing 100μl of culture medium. We measured the absorbance at 490nm using a 96-well plate reader after 2 hours incubation of cells with MTS agent.

Laser treatment

Prior to the cell culture, the sterile glass coverslips were coated with fibronectin 0.75% in PBS for at least one hour to enhance cell adhesion. We seeded MDA-MB-231 cells onto these coverslips in a 12-well plate. Cells were incubated with AuNRs in a similar method as for imaging AuNRs internalization. After incubation time, the AuNRs suspensions were removed, and the cells were washed once with PBS. To prepare the sample of MDA-MB-231 cells blended with AuNRs-embedded cells, we first cultured cells with and without AuNRs separately, trypsinized, and mixed these two populations with a 2:1 ratio. We irradiated cells with an Nd:YAG 1064nm pulsed laser (1 pulse, pulse duration of 20ns, beam width of 3mm at the coverslip plane) in the fluence range of 0.7 – 5J/cm^2. Laser irradiation at 1064nm has previously been reported to result in deeper tissue penetration in comparison to near-infrared I wavelengths in mice.[23] We noted that the absorption peak of AuNRs at 788nm and laser irradiation at 1064nm would only result in 25% absorption in comparison to that of at 788nm. However, this off-resonance absorption at 1064nm can be compensated by increasing laser fluence while maintaining a significant margin between triggering cell death with and without AuNRs[26] and gaining a deep penetration depth in vivo. Moreover, several studies have shown that nanosecond pulses could generate bubbles in the range of submicron to microns size,[54] which are large enough to trigger membrane disruption.[25,55] Immediately following laser treatment, cells are stained with the viability/cytotoxicity kit (Invitrogen) for 30 minutes at 37°C in a humidified, 5% CO_2 atmosphere. After staining, cells were washed with PBS and imaged with a two-photon microscope in a similar setting as for imaging AuNRs internalization. To quantify cell death, we sampled five tiles of images in the center of the laser beam of each sample and count the number of live and dead cells. Percentage of cell death is calculated as the ratio of number of red cells over total number of cells.

Bubble imaging

For observation of vapor bubbles around AuNRs in cells, we set up an inverted microscope, as shown in Figure 4a. The 1064nm excitation laser beam was focused to a spot of 60μm diameter (FWHM) on the sample through the microscope objective (Olympus, 40x). Laser energy was adjusted to a fluence of 3J/cm^2 at the sample plane. The images of bubbles were captured by a high-speed camera (Photron) at 25,000fps. To quantify bubbles' lifetime, we monitored the mean intensity of bubbles pixels versus time and fit the intensity to a biexponential decay function to determine the time when the intensity reduces 1/e (67%) of its peak-to-plateau difference. The diffraction limit of the system is calculated using Abbe's diffraction formula for lateral resolution as follows:

$$d = \frac{\lambda}{2NA}$$

Assuming wavelength λ = 500 nm and NA of the system as 0.95, the resolution is calculated as 0.26 μm.

Measurement of DAMPs

To characterize the release of DAMPs in the extracellular environment after laser irradiation, we seeded and grew MDA-MB-231 and 4T1 cells in 12-well plates until 80% confluence. Cells were incubated with 35 μg/ml Mutab-coated AuNRs in 1 ml culture medium for 6 hours. Each well was then irradiated at 3 J/cm^2 with 64 spots (8 columns x 8 rows) via LabVIEW control of motorized x-y translation stages and the 1064nm laser. The area of cells irradiated with laser is around 50% of a well or around 2 cm^2. Doxorubicin treatment was used as the positive control (1 μg/ml for MDA-MB-231 and 10 μg/ml for 4T1 cells). The supernatant was collected to protein low-bind tubes and centrifuged at 10,000rpm and 4 minutes to separate the residuals to the end of the tubes. We used HMGB1 ELISA kit (Chrondex), HSP70 ELISA kit (R&D System), and ATP Bioluminescent kit (Sigma-Aldrich) following suppliers' protocols to measure the amount of the DAMPs released in the extracellular environment.

Dendritic cell activation

Bone marrow-derived dendritic cells (DCs) from BALB/c mice (Charles River Laboratories) housed in semi-barrier facilities were cultured as per the Lutz method, with the addition of IL-4.[47–49] Briefly, femurs and tibias were isolated and sterilized. Bone marrow was flushed from the femur and tibias using sterile PBS. Cells were centrifuged prior to erythrolysis with ACK lysing buffer (Lonza). The reaction was stopped by the addition of PBS, and cells were centrifuged again. Bone marrow cells were resuspended in RPMI 1640 medium, ATCC modification (Gibco) containing 10% heat-inactivated FBS (Gibco), 100 U/ml penicillin (Caisson Labs), 100 μg/ml streptomycin (Caisson Labs), passed through a 70 μm cell strainer and counted. Cells were diluted to reach a concentration of 2×10^5 cells/ml and were supplemented with 50 μM 2-mercaptoethanol (Sigma-Aldrich), 20 ng/ml GM-CSF (PeproTech), and 10 ng/ml IL-4 (PeproTech), and 6 ml of the resulting mixture was added to 60 mm tissue-culture treated dishes (Falcon, Corning). On day 3, 6 ml of complete media containing all supplements was added to each dish. On days 6 and 8, 6 ml of media was removed, centrifuged to retain cells,

and resuspended in 6 ml of fresh media with supplements prior to distribution to the original dishes. On day 10, non-adherent cells were collected by gentle pipetting. Cells were counted for experiments, and 0.5 x 106 cells were plated to a 6-well plate with 10 ng/ml GM-CSF prior to treatment. Separately, 4T1 cells were seeded and grown on transwells (Corning, 0.4 μm PET membrane, 23.1 mm) until confluence and incubated with 35 μg/ml Mutab-coated AuNRs in 2 ml culture medium for 6 hours. After that, the AuNRs suspension was removed, and 4T1 cells were washed with PBS once before moving to be cocultured with DCs in a 6-well plate. The 4T1 cells were irradiated in a similar method as for the characterization of DAMPs release. The second irradiation is 12 hours after the first irradiation. Twenty-four hours after the first laser irradiation, DCs were stained with anti-CD11c FITC, anti-CD86 PE and anti-CD80 647 (Thermofisher), and then sorted by flow cytometry (BD Fortesa). Lipopolysaccharide (LPS, Sigma) at 1 μg/ml was used as positive control. Gating strategy for dendritic cell activation was described in Figure S1. We first gated out the debris population with low forward and side scattering. We then selected the singlets with a linear correlation between forward-scattering height and area. We used a viability dye (eFluor 506, Thermo Fisher) to gate the live cell population that did not fluoresce at 506 nm. We next selected the positive expressed Cd11c cells (FITC, Thermo Fisher) as dendritic cells population. Lastly, the positive expressed Cd86 (PE, Thermo Fisher) and MHCII (AF647, Thermo Fisher) cells were labelled as mature dendritic cells. All gates with fluorophores were defined by fluorescence minus one (FMO) control samples that were used to determine the cut-off point between background fluorescence and positive populations in multi-color immunofluorescent experiments.

Statistical Analysis

To compare the difference between groups, we used R (Rstudio 2018) to perform analysis variance (ANOVA) in combination with the Tukey test as a post-hoc analysis.

Conclusions

We observed a single 1064nm nanosecond laser pulse in combination with gold nanorods eradicates breast cancer cells and induces immunogenic cell death. We detected cell death from membrane disruption after laser irradiation, which only happened in cells with nanorods, while neighboring cells without nanorods were left intact. We also observed bubbles and discrete cellular damage around the bubbles as the result of nanorod-laser interaction. We demonstrated that DAMPs released in the extracellular environment are enhanced in the laser treatment group. With the presence of DAMPs released from laser irradiation, dendritic cell activation was also increased. Overall, we determined that nanosecond pulsed laser irradiation provided a fast and highly specific approach to eradicate tumor cells and induce markers of immunogenic cell death. This study provides supporting experimental evidence of the concept that laser nanobubbles trigger immunogenic cell death in cancer cells and shows the potential of reprogramming tumor environment for enhancing immunotherapy .

Conflicts of interest

There are no conflicts to declare.

Author contributions

Conceptualization: J.W. Tunnell, H.T.M. Nguyen
Formal analysis: H.T.M. Nguyen, N. Katta, J.A. Widman
Investigation: H.T.M. Nguyen, N. Katta, J.A. Widman, E. Takematsu, X. Feng, S. H. Torres
Methodology: H.T.M. Nguyen
Materials and equipment: J.W. Tunnell, J.W. Tunnell, T.E. Milner, L.J. Suggs, A.B. Baker, T. Betancourt
Writing – original draft: H.T.M. Nguyen, J.A. Widman
Writing – review & editing: J.W. Tunnell, T.E. Milner, L.J. Suggs, A.B. Baker, T. Betancourt

Acknowledgements

The work was supported by the Cancer Prevention and Research Institute of Texas (CPRIT RP130702), Texas Health Catalyst, and Texas 4000. The authors gratefully acknowledge funding through the American Heart Association (17IRG33410888), the DOD CDMRP (W81XWH-16-1-0580; W81XWH-16-1-0582) and the National Institutes of Health (1R21EB023551-01; 1R21EB024147-01A1; 1R01HL141761-01) to ABB. The authors sincerely appreciate the fruitful discussion with professor Preston Wilson and Dr. Emil Sobol on the topic of nanobubble dynamics and discussion with professor Rongze Lu on the subject of dendritic cell activation. We would like to thank Dr. Adrian Spencer and Daniel Chavarria from Baker lab for help with the MDA-MB-231 cell line; Scott Jenney and Dr. Bharadwaj Muralidharan from Milner lab for assistance with the optical fibers and alignment; Dr. Kabir Dhada from Suggs lab for support with the Nd: YAG 1064 nm laser.

References

1 M. Maio, J.-J. Grob, S. Aamdal, I. Bondarenko, C. Robert, L. Thomas, C. Garbe, V. Chiarion-Sileni, A. Testori, T.-T. Chen, M. Tschaika and J. D. Wolchok, *J. Clin. Oncol.*, 2015, **33**, 1191–1196.
2 F. S. Hodi, S. J. O'Day, D. F. McDermott, R. W. Weber, J. A. Sosman, J. B. Haanen, R. Gonzalez, C. Robert, D. Schadendorf, J. C. Hassel, W. Akerley, A. J. M. van den Eertwegh, J. Lutzky, P. Lorigan, J. M. Vaubel, G. P. Linette, D. Hogg, C. H. Ottensmeier, C. Lebbé, C. Peschel, I. Quirt, J. I. Clark, J. D. Wolchok, J. S. Weber, J. Tian, M. J. Yellin, G. M. Nichol, A. Hoos and W. J. Urba, *N. Engl. J. Med.*, 2010, **363**, 711–723.
3 S. C. Wei, C. R. Duffy and J. P. Allison, *Cancer Discovery*, 2018, **8**, 1069–1086.
4 R. Nanda, L. Q. M. Chow, E. C. Dees, R. Berger, S. Gupta, R. Geva, L. Pusztai, K. Pathiraja, G. Aktan, J. D. Cheng, V. Karantza and L. Buisseret, *J. Clin. Oncol.*, 2016, **34**, 2460–2467.
5 P. Sharma and J. P. Allison, *Science*, 2015, **348**, 56–61.
6 P. M. Forde, J. E. Chaft, K. N. Smith, V. Anagnostou, T. R. Cottrell, M. D. Hellmann, M. Zahurak, S. C. Yang, D. R. Jones, S. Broderick, R. J. Battafarano, M. J. Velez, N. Rekhtman, Z. Olah, J. Naidoo, K. A. Marrone, F. Verde, H. Guo, J. Zhang, J. X. Caushi, H. Y. Chan,

J.-W. Sidhom, R. B. Scharpf, J. White, E. Gabrielson, H. Wang, G. L. Rosner, V. Rusch, J. D. Wolchok, T. Merghoub, J. M. Taube, V. E. Velculescu, S. L. Topalian, J. R. Brahmer and D. M. Pardoll, *N. Engl. J. Med.*, 2018, **378**, 1976–1986.

7 O. Kepp, L. Senovilla, I. Vitale, E. Vacchelli, S. Adjemian, P. Agostinis, L. Apetoh, F. Aranda, V. Barnaba, N. Bloy, L. Bracci, K. Breckpot, D. Brough, A. Buqué, M. G. Castro, M. Cirone, M. I. Colombo, I. Cremer, S. Demaria, L. Dini, A. G. Eliopoulos, A. Faggioni, S. C. Formenti, J. Fučíková, L. Gabriele, U. S. Gaipl, J. Galon, A. Garg, F. Ghiringhelli, N. A. Giese, Z. S. Guo, A. Hemminki, M. Herrmann, J. W. Hodge, S. Holdenrieder, J. Honeychurch, H.-M. Hu, X. Huang, T. M. Illidge, K. Kono, M. Korbelik, D. V. Krysko, S. Loi, P. R. Lowenstein, E. Lugli, Y. Ma, F. Madeo, A. A. Manfredi, I. Martins, D. Mavilio, L. Menger, N. Merendino, M. Michaud, G. Mignot, K. L. Mossman, G. Multhoff, R. Oehler, F. Palombo, T. Panaretakis, J. Pol, E. Proietti, J.-E. Ricci, C. Riganti, P. Rovere-Querini, A. Rubartelli, A. Sistigu, M. J. Smyth, J. Sonnemann, R. Spisek, J. Stagg, A. Q. Sukkurwala, E. Tartour, A. Thorburn, S. H. Thorne, P. Vandenabeele, F. Velotti, S. T. Workenhe, H. Yang, W.-X. Zong, L. Zitvogel, G. Kroemer and L. Galluzzi, *OncoImmunology*, 2014, **3**, e955691.

8 G. Kroemer, L. Galluzzi, O. Kepp and L. Zitvogel, *Annual Review of Immunology*, 2013, **31**, 51–72.

9 D. V. Krysko, A. D. Garg, A. Kaczmarek, O. Krysko, P. Agostinis and P. Vandenabeele, *Nature Reviews Cancer*, 2012, **12**, 860–875.

10 Y. Li, S. Gong, W. Pan, Y. Chen, B. Liu, N. Li and B. Tang, *Chemical Science*, 2020, **11**, 7429–7437.

11 D. P. O'Neal, L. R. Hirsch, N. J. Halas, J. D. Payne and J. L. West, *Cancer Letters*, 2004, **209**, 171–176.

12 L. R. Hirsch, R. J. Stafford, J. A. Bankson, S. R. Sershen, B. Rivera, R. E. Price, J. D. Hazle, N. J. Halas and J. L. West, *Proc. Natl. Acad. Sci. U.S.A.*, 2003, **100**, 13549–13554.

13 C. Loo, A. Lin, L. Hirsch, M.-H. Lee, J. Barton, N. Halas, J. West and R. Drezek, *Technol. Cancer Res. Treat.*, 2004, **3**, 33–40.

14 Y. Li, X. Zhang, X. Liu, W. Pan, N. Li and B. Tang, *ACS Appl. Bio Mater.*, 2020, **3**, 8321–8337.

15 S. Toraya-Brown, M. R. Sheen, P. Zhang, L. Chen, J. R. Baird, E. Demidenko, M. J. Turk, P. J. Hoopes, J. R. Conejo-Garcia and S. Fiering, *Nanomedicine*, 2014, **10**, 1273–1285.

16 B. Frey, E.-M. Weiss, Y. Rubner, R. Wunderlich, O. J. Ott, R. Sauer, R. Fietkau and U. S. Gaipl, *Int J Hyperthermia*, 2012, **28**, 528–542.

17 J. J. Skitzki, E. A. Repasky and S. S. Evans, *Curr Opin Investig Drugs*, 2009, **10**, 550–558.

18 S. K. Calderwood, J. R. Theriault and J. Gong, *Int J Hyperthermia*, 2005, **21**, 713–716.

19 A. J. Moy and J. W. Tunnell, *Advanced Drug Delivery Reviews*, 2017, **114**, 175–183.

20 Y. Li, X. Liu, W. Pan, N. Li and B. Tang, *Chemical Communications*, 2020, **56**, 1389–1392.

21 A. S. Bear, L. C. Kennedy, J. K. Young, S. K. Perna, J. P. Mattos Almeida, A. Y. Lin, P. C. Eckels, R. A. Drezek and A. E. Foster, *PLoS ONE*, 2013, **8**, e69073.

22 Q. Chen, L. Xu, C. Liang, C. Wang, R. Peng and Z. Liu, *Nature Communications*, 2016, **7**, 13193.

23 Y. Ma, Y. Zhang, X. Li, Y. Zhao, M. Li, W. Jiang, X. Tang, J. Dou, L. Lu, F. Wang and Y. Wang, *ACS Nano*, 2019, **13**, 11967–11980.

24 X. Huang, B. Kang, W. Qian, M. A. Mackey, P. C. Chen, A. K. Oyelere, I. H. El-Sayed and M. A. El-Sayed, *Journal of Biomedical Optics*, 2010, **15**, 058002.

25 C. M. Pitsillides, E. K. Joe, X. Wei, R. R. Anderson and C. P. Lin, *Biophysical Journal*, 2003, **84**, 4023–4032.

26 C. Boutopoulos, E. Bergeron and M. Meunier, *Journal of Biophotonics*, 2016, **9**, 26–31.

27 T. Patino, U. Mahajan, R. Palankar, N. Medvedev, J. Walowski, M. Münzenberg, J. Mayerle and M. Delcea, *Nanoscale*, 2015, **7**, 5328–5337.

28 K. Schnarr, R. Mooney, Y. Weng, D. Zhao, E. Garcia, B. Armstrong, A. J. Annala, S. U. Kim, K. S. Aboody and J. M. Berlin, *Advanced Healthcare Materials*, 2013, **2**, 976–982.

29 F. Ratto, S. Centi, C. Avigo, C. Borri, F. Tatini, L. Cavigli, C. Kusmic, B. Lelli, S. Lai, S. Colagrande, F. Faita, L. Menichetti and R. Pini, *Advanced Functional Materials*, 2016, **26**, 7178–7185.

30 A. M. Alkilany, P. K. Nagaria, C. R. Hexel, T. J. Shaw, C. J. Murphy and M. D. Wyatt, *Small*, 2009, **5**, 701–708.

31 T. S. Hauck, A. A. Ghazani and W. C. W. Chan, *Small*, 2008, **4**, 153–159.

32 Y. Qiu, Y. Liu, L. Wang, L. Xu, R. Bai, Y. Ji, X. Wu, Y. Zhao, Y. Li and C. Chen, *Biomaterials*, 2010, **31**, 7606–7619.

33 H. T. M. Nguyen, N. Katta, J. A. Widman, L. J. Suggs, T. E. Milner and J. W. Tunnell, in *Biophotonics Congress: Biomedical Optics 2020 (Translational, Microscopy, OCT, OTS, BRAIN) (2020), paper TTu1B.5*, Optical Society of America, 2020, p. TTu1B.5.

34 A. Siems, S. a. L. Weber, J. Boneberg and A. Plech, *New J. Phys.*, 2011, **13**, 043018.

35 E. Lukianova-Hleb, Y. Hu, L. Latterini, L. Tarpani, S. Lee, R. A. Drezek, J. H. Hafner and D. O. Lapotko, *ACS Nano*, 2010, **4**, 2109–2123.

36 M. Kitz, S. Preisser, A. Wetterwald, M. Jaeger, G. N. Thalmann and M. Frenz, *Biomedical Optics Express*, 2011, **2**, 291.

37 P. S. Epstein and M. S. Plesset, *J. Chem. Phys.*, , DOI:https://doi.org/10.1063/1.1747520.

38 S. Ljunggren and J. C. Eriksson, *Colloids and Surfaces A: Physicochemical and Engineering Aspects*, 1997, **129–130**, 151–155.

39 L. Zhang, H. Chen, Z. Li, H. Fang and J. Hu, *Science in China Series G: Physics, Mechanics and Astronomy*, 2008, **51**, 219–224.

40 R. Parmarand and S. K. Majumder, *ChemXpress*, 2016, **9**, 046–054.

41 É. Boulais, R. Lachaine and M. Meunier, *Nano Letters*, 2012, **12**, 4763–4769.

42 A. Dutta and A. S. Popel, *Journal of Theoretical Biology*, 1995, **176**, 433–445.

43 S. L. Richardson, A. Hulikova, M. Proven, R. Hipkiss, M. Akanni, N. B. A. Roy and P. Swietach, *PNAS*, 2020, **117**, 10067–10078.

44 A. Philipp and W. Lauterborn, *Journal of Fluid Mechanics*, 1998, **361**, 75–116.

45 E. A. Brujan, G. S. Keen, A. Vogel and J. R. Blake, *Physics of Fluids*, 2001, **14**, 85–92.

46 L. Bezu, L. C. Gomes-de-Silva, H. Dewitte, K. Breckpot, J. Fucikova, R. Spisek, L. Galluzzi, O. Kepp and G. Kroemer, *Frontiers in Immunology*, , DOI:10.3389/fimmu.2015.00187.

47 M. B. Lutz, N. Kukutsch, A. L. J. Ogilvie, S. Rößner, F. Koch, N. Romani and G. Schuler, *Journal of Immunological Methods*, 1999, **223**, 77–92.

48 J. Helft, J. Böttcher, P. Chakravarty, S. Zelenay, J. Huotari, B. U. Schraml, D. Goubau and C. Reis e Sousa, *Immunity*, 2015, **42**, 1197–1211.

49 M. B. Lutz, *Immunobiology*, 2004, **209**, 79–87.

50 J. A. Villadangos, P. Schnorrer and N. S. Wilson, *Immunol. Rev.*, 2005, **207**, 191–205.

51 A. Sapoznikov, Y. Pewzner-Jung, V. Kalchenko, R. Krauthgamer, I. Shachar and S. Jung, *Nature Immunology*, 2008, **9**, 388–395.
52 V. P. Pattani, J. Shah, A. Atalis, A. Sharma and J. W. Tunnell, *Journal of Nanoparticle Research*, , DOI:10.1007/s11051-014-2822-3.
53 J. Park and J. W. Tunnell, *Optics Express*, 2008, **16**, 1590.
54 D. O. Lapotko, E. Lukianova and A. A. Oraevsky, *Lasers in Surgery and Medicine*, 2006, **38**, 631–642.
55 S. Peeters, M. Kitz, S. Preisser, A. Wetterwald, B. Rothen-Rutishauser, G. N. Thalmann, C. Brandenberger, A. Bailey and M. Frenz, *Biomed. Opt. Express*, 2012, **3**, 435–446.